Au(111)-Based Nanotemplates by Gd Alloying

Martina Corso,[†,*] Laura Fernández,[†] Frederik Schiller,[‡] and José Enrique Ortega[†,‡,§,*]

[†]Donostia International Physics Center (DIPC), Paseo Manuel de Lardizábal 4, 20018 San Sebastián, Spain, [‡]Centro de Física de Materiales (CSIC-UPV-EHU) and Material Physics Center (MPC), Manuel de Lardizábal 4, 20018 San Sebastián, Spain, and [§]Departamento de Física Aplicada I, Universidad del País Vasco, Plaza Oñate 2, 20018 San Sebastián, Spain

ABSTRACT A new class of nanostructured templates is obtained by submitting Au(111) films to high-temperature vapor deposition of Gd in ultrahigh vacuum. In a low coverage regime, Gd atoms are embedded in the topmost Au layer, inducing a structural transformation of the *herringbone reconstruction* to create a network of *trigons*. At higher dose, the reactive deposition of Gd leads to the formation of an atomically perfect $GdAu_2$ surface compound characterized by a long-range periodic Moiré pattern. Both the trigon and Moiré lattices are highly ordered nanostructures, which turned out to be robust templates to grow metal nanodots. As a test example, Co was deposited at room temperature, forming uniform dots that faithfully arrange by following the underlying trigons or Moiré periodicity. For the latter, one can achieve nanodot arrays that exhibit record areal density.

KEYWORDS: Gd−Au nanostructures · gold · data storage · nanotemplate · self-assembly

The herringbone reconstruction in Au(111) is among the most studied and exploited in surface science. Nowadays, there is a great interest to use such prepatterned surface as a template to organize molecules or metallic clusters in view of their eventual use in nanoelectronics, information storage, and nanocatalysis.[1,2] Au can be easily grown as a thin crystalline film in a number of handy substrates, such as glass, mica, or Si(111).[3−5] Therefore, the Au(111) reconstructed surface is an attractive, unique, and versatile substrate suitable for many kinds of nanotechnological applications and investigations with different experimental techniques.

Here we present an easy way to tune the Au herringbone structure and periodicity by the addition of external atomic species. In particular, we report for the first time on a detailed characterization of the growth of a rare earth metal, Gd, on Au(111). The exposure at high temperature (550 K) to low amounts of Gd transforms the herringbone pattern and induces the formation of a highly ordered network of *trigons*. An increased exposure to Gd in the same growth conditions leads to the creation of a stable $GdAu_2$ surface compound. We show how these peculiar Gd−Au superstructures, as the Au herringbone, are able to host ordered arrays of isolated metal nanodots, as found in the case of Co.

RESULTS AND DISCUSSION

Herringbone Reconstruction of Au(111). The surface reconstruction of Au(111), known as "herringbone (HB)", "chevron", or "22 × $\sqrt{3}$" shown in Figure 1, was studied intensively both theoretically and experimentally, especially with scanning tunneling microscopy (STM)[6] and diffraction techniques.[7,8] In order to understand how this complex structure evolves when alloying with Gd, we briefly review its atomic arrangement. In Figure 1, we show large size high-resolution STM images of the Au(111) surface, which allows us to determine the key features of the reconstruction and define at the atomic level, for the first time, the entire surface unit cell.

The 22 × $\sqrt{3}$ reconstruction, which occurs spontaneously at room temperature (rt), has its origin in an uniaxial contraction of ~4.4% of the surface layer with respect to the bulk.[9] In fact, the surface stresses created by cleavage of the bulk metal are minimized by reducing the surface gold−gold interatomic separations. Along the close-packed [1$\bar{1}$0] direction, 23 surface atoms occupy 22 substrate positions, resulting in the formation of alternating areas where surface atoms occupy *fcc* or *hcp* sites of the underlying bulk lattice. We measure an average value for the nearest neighbor Au−Au distances (d_{Au-Au}) in the topmost layer of $d_{Au-Au} = 2.82 \pm 0.25$ Å and a unit cell size of ~65 × 4.88 Å^2. The width of *fcc*-like regions, energetically the most stable, is larger than that of the *hcp*-like due to the

*Address correspondence to martina_corso@ehu.es, enrique.ortega@ehu.es.

Received for review October 2, 2009 and accepted February 1, 2010.

Published online February 10, 2010. 10.1021/nn901345s

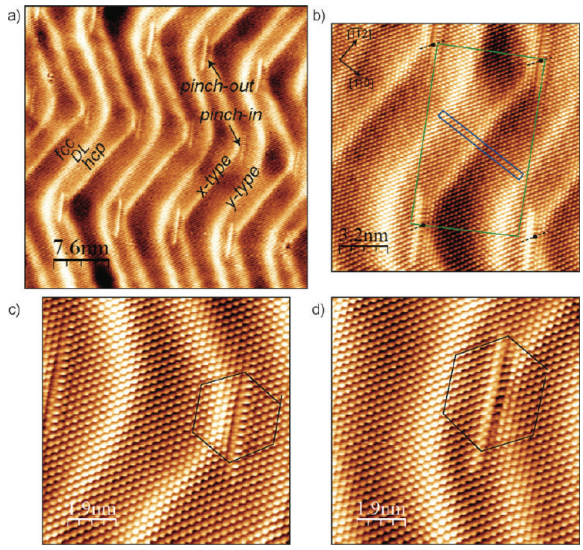

Figure 1. High-resolution STM images of the atomic structure of the reconstructed Au(111) surface (I_t = 3 nA, V_s = −0.1 V), no filters are applied. (a) Large-scale image where domains with *fcc* and *hcp* stacking separated by discommensuration lines (DL) as well as the two different types of elbows (*x* and *y*) and dislocations (pinch-in, pinch-out) are visible. (b) Black points indicate the exact position at which dislocations occur. The smaller unit cell (blue) defines the (23 × $\sqrt{3}$)d_{Au-Au}, while the large rectangle (green) corresponds to half of the unit cell defined by equivalent dislocations. Pinch-in (c) and pinch-out (d) dislocations with a missing atom and extra atom, respectively, as indicated by the Burger circuits.

modulation in the surface stress.[10] Such regions are separated by discommensuration lines (DL), the brightest areas in Figure 1, oriented in the [$\bar{1}\bar{1}$2] directions, where some gold atoms, forced to occupy unfavorable bridge-like positions, are lifted with respect to the surface plane giving rise to the 0.2 ± 0.05 Å corrugation observed by STM.

Due to the three-fold symmetry of the (111) surface, three possible 22 × $\sqrt{3}$ domains can occur along the three allowed close-packed directions. The periodic repetition of two joint equivalent 22 × $\sqrt{3}$ domains, which favors a more isotropic surface stress relief, creates the herringbone-type pattern. The DL form zigzag lines that bend ±120° at the borders between adjacent 22 × $\sqrt{3}$ areas. Two types of alternating DL exist in the HB: one that contains a point dislocation at every "elbow" where the ridges bend (*x*-type) and the other free from any dislocation (*y*-type),[11,12] as indicated in Figure 1a. On *x*-type boundary DL, two kinds of dislocations alternate: one with a missing atom called "pinch-in" (Figure 1c) and one with an extra atom called "pinch-out" (Figure 1d). In Figure 1c,d, Burger circuits are pictured to identify the two types of dislocations. Equivalent dislocation points define a rectangular surface unit cell larger than the (23 × $\sqrt{3}$)d_{Au-Au}. We are able to assign its exact size from a careful analysis of our large-scale atomically resolved STM images. This large unit cell covers (~14$\sqrt{3}$ × 82)d_{Au-Au}, which corresponds to ~68 × 231 Å^2. Half of this unit cell and its orientation with respect to the principal one are indicated in Figure 1b.

Low Coverage Gd Growth on Au(111). Experiments demonstrated that any alteration of the interaction strength between surface and bulk atoms can influence the morphology of the Au(111) reconstruction. In particular, changes in the HB have been observed as a result of temperature increase from rt to ~430 K,[13] by applying strong localized electric field (from an STM tip), which can partially lift the reconstruction,[9] by modifying the surface atomic density as has been done with exposure to metals such as Al,[14] to alkaline metals,[15,16] or by self-assembly of Azure A molecules.[17] The latter method is particularly attractive as a way of smoothly tuning the nanopattern. Here we use Gd, a rare earth metal, as guest species to modify the HB.

Gd was evaporated by molecular beam epitaxy on the clean Au(111) substrate with a deposition rate of 2 Å/min, as estimated from a quartz microbalance. We found that for high-temperature depositions (500−600 K substrate temperature) Gd atoms easily diffuse inside the Au bulk. Therefore, we are not able to quantify the exact amount of Gd in the whole sample, but we can easily estimate from STM images the quantity of Gd atoms in the surface layer.

Figure 2a presents the Au(111) surface after ~10 s gadolinium deposition at a substrate temperature of 550 K. After incorporation of 4% of Gd atoms, the HB structure is transformed: the *y*-type DL become straighter, while the *x*-type DL widen, forming a network of "triangles". This atomic arrangement in the "distorted HB" allows Au atoms to cover wider *fcc* areas. The large-scale HB unit cell shrinks to (73 × 110) ± 5 Å^2.

An increase of the Gd exposure (20−30 s) with the same deposition conditions causes the formation of a highly regular network of trigons (Figure 2b). Instead of the zigzag pattern characteristic of the HB phase, the DL form wavy triangles. The resulting hexagonal structure has a periodicity of 90 ± 6 Å. The corrugation of the

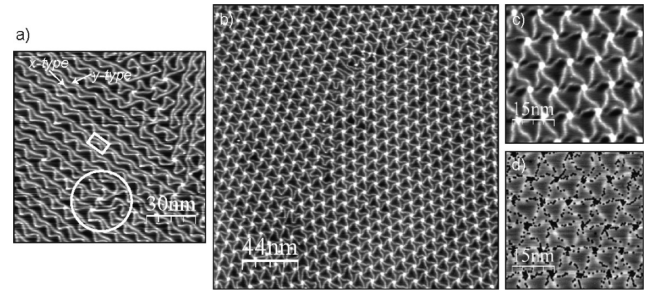

Figure 2. STM images measured after exposing a hot (550 K) Au(111) surface to ~10 s of Gd in (a) and ~20 s in (b−d). (a) Distorted herringbone whose large unit cell is identified by the rectangle. A few trigon units are highlighted by the circle. (b) Two ordered domains of trigons. (c) Detailed structure of the trigons network, where their whorl-like appearance is clearly visible. (d) Same structure in (c) is imaged with a different STM tip resolution, revealing Gd atoms (black). (a−c) I_t = 0.1 nA, V_s = −1 V; (d) I_t = 0.3 nA, V_s = −1 V.

lines is the same as that in the HB (0.2 ± 0.05 Å), while the network nodes are higher on the surface (0.5 ± 0.05 Å). STM images taken under particular tip or tunneling conditions show that Gd atoms integrate in the Au lattice, thus inducing a further contraction of the surface layer. As visible in Figure 2d, Gd is incorporated in the DL and in their junction points, the least favorable adsorption sites for Au atoms. From the analysis of these STM images, we find that Gd atoms occupy 6.5% of the surface. This value is in good agreement with the results of simulations for the Pt(111) surface.[18] In fact, also on that surface, a similar network of trigons forms by placing Pt(111) in a supersaturated Pt vapor or by heating it above 1330 K.[19] Wavy triangles similar to those in Gd/Au(111) are found for an excess atomic density in the Pt(111) surface layer between 4 and 6.8% and for a 0.14° rotation of the top Pt layer with respect to the substrate.[18] The authors identify the larger triangles as *fcc* areas separated from the smaller *hcp* triangular domains by DL with atoms at bridge positions. The bright vertices, where six DL join, are due to atoms sitting *on top* sites. The whorl-like appearance of the trigons is due to a slight rotation of the surface layer. The same atomic site occupation was assigned for the analogous surface reconstruction experimentally observed for Na/Au(111).[15,16] In that case, the network of trigons, formed after annealing to 600 K of a Au(111) surface covered by 0.23 ML of Na, consists of a distorted hexagonal (DHEX) lattice of DL with a periodicity between 70 and 95 Å, similar to the one found for Gd but generally more irregular. A smaller periodicity of 55−60 Å was found for the Al-induced Au(111) DHEX reconstruction formed at a lower annealing temperature (450 K).[14]

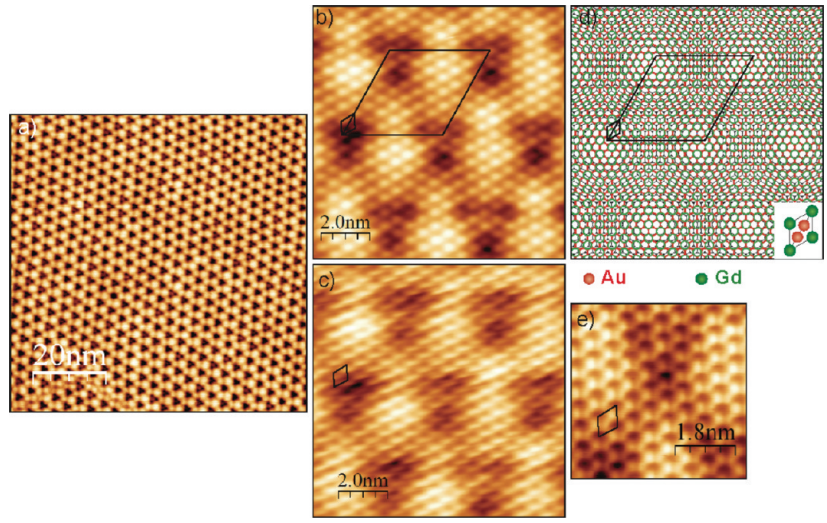

Figure 3. (a) STM image of the $GdAu_2$ surface compound, characterized at large scale by a hexagonal Moiré pattern. Its atomic structure is resolved in (b), (c), and (e). Two different atomic contrasts can be distinguished: in (b), one atomic species arranged in a hexagonal lattice is imaged as a protrusion, while in (c) and (e), only the charge surrounding it appears. As visible in (e), such a contrast is due to six atoms. (d) Atomic model of the $GdAu_2$ surface structure where the green circle corresponds to Gd atoms and red circles to Au atoms. The small hexagonal unit cell in the model matches with one atomic species (as in (b)), while the large unit, rotated 30° with respect to the small one, highlights the Moiré superstructure. (a) I_t = 0.4 nA, V_s = 1 V; (b) I_t = 0.3 nA, V_s = −1.5 V; (c) I_t = 0.3 nA, V_s = −0.04 V; (e) I_t = 2 nA, V_s = −1 V.

A hint on the formation of the trigon phase is given by the observation of the Au(111) surface at low Gd coverages. In Figure 2a, a few trigons are included in a circular area; there, trigons form by the fusion of three triangular units of the distorted HB. Each one of these triangular units contains a point dislocation at its vertices,[20] as it is known for the U turns of the dislocation lines observed in HB.[6] The node of a trigon forms where three triangles join and the three corresponding dislocations annihilate, leaving the trigon phase free from point dislocations and energetically more stable as suggested for Pt(111) and Na/Au(111).[19]

High Coverage Gd Growth on Au(111). A novel equilibrium surface phase forms when the Au(111) surface is exposed to even higher amounts (2.5 min) of Gd at 550 K. Figure 3a shows typical STM images of this Gd−Au structure. At first sight, it appears as a network of triangles connected by dark lines, a contrast already observed in several dislocation networks as Ag/Cu(111),[21,22] Au/Ni(111),[23] or the AgAu/Ru(0001) alloy.[24] On the contrary to those systems, we interpret the Gd−Au motif as a simple Moiré pattern. In atomically resolved STM images, two contrasts can be identified, as shown in Figure 3b,c. At voltages with values far from the Fermi level (E_F) (V_s = −1.5 V in Figure 3b), only one atomic species is resolved which forms a continuous hexagonal surface layer with a nearest neighbor distance of d_{atoms} = 5.5 ± 0.3 Å, much larger than the typical in-plane Gd(0001) interatomic distance of 3.64 Å and the atomic spacing on the Au(111) surface. On the other side, for a sample bias ranging from V_s = ±0.1 to V_s = ±0.01 V, such atomic species are imaged as depressions (Figure 3c). With a closer look, as in Figure 3e, we can identify the electronic charge surrounding each depression as due to six atoms with an interatomic distance of 2.9 ± 0.25 Å. The Moiré overstructure is 30° rotated to the atomic layer (Figure 3b) and has a periodicity of 38 ± 2 Å corresponding to $d_{Moiré} = 4\sqrt{3}d_{atoms}$.

Low-energy electron diffraction patterns (LEED) allow one to identify the relation between the Gd−Au structure and the Au substrate (Figure 4). In Figure 4b, where the Au(111) surface is partially covered by Moiré, we can clearly see that the overstructure has the same orientation as the Au(111) substrate. Its periodicity is close to 13 in-plane Au(111) lattice units, as results from exact simulations of LEED patterns as the one in Figure 4b recorded at 63 eV. Therefore, the atomic lattice seen in STM (Figure 3b) is 30° rotated to the Au substrate.

We investigated the Gd−Au surface with X-ray photoelectron spectroscopy (XPS). In order to enhance sur-

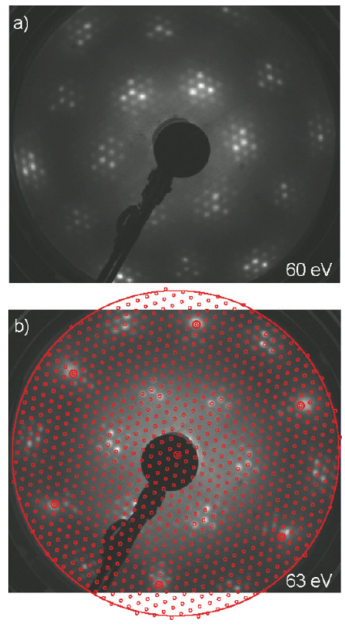

Figure 4. LEED patterns of a Au(111) surface fully (a) and partially (b) covered by the Gd−Au structure. In (b), the recorded image is overlaid by a simulated pattern. The large circles correspond to substrate spots, while the small ones correspond to the Gd−Au Moiré superstructure defined by (13 × 13) Au units. The simulation has been performed with a beam energy of 63 eV corrected for the measured sample work function of 4.7 eV, and the pattern is projected on a spherical LEED screen of radius of 52 mm and a sample screen distance of 54 mm.

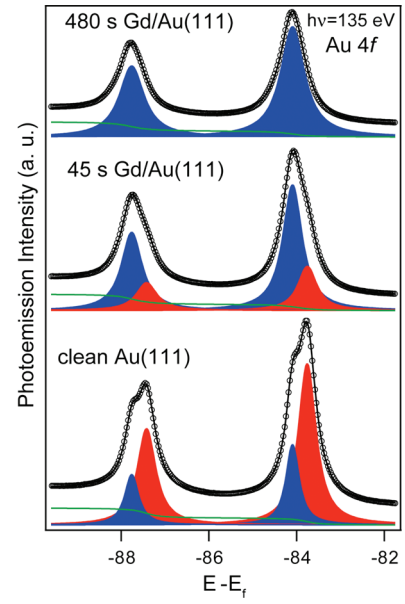

Figure 5. XPS measurements of the Au 4f emissions (photon energy $h\nu$ = 135 eV) carried out on a clean Au(111) surface, a partially covered Au(111) with $GdAu_2$ compound (45 s Gd evaporation), and a completely covered Au(111) with the $GdAu_2$ compound (480 s Gd evaporation) as indicated. For clean Au, each peak consists on a doublet structure that results from the surface (red) and bulk (blue) emissions. After 45 s of Gd deposition, the intensity of the surface component is largely attenuated while the nonsurface emissions increase. After 480 s Gd deposition, the surface component is totally suppressed and the total emissions amount to 2/3 of the original Au(111) 4f emissions.

face sensitivity in Au 4f core levels, the photon energy was tuned to 135 eV. Figure 5 shows the result of the measurements. For clean Au, one observes a main splitting due to the spin−orbit interaction into the $4f^{7/2}$ ($E - E_F \sim -84$ eV) and the $4f^{5/2}$ ($E - E_F \sim -88$ eV) components. Each of the two peaks consists of a doublet structure, arising from the surface (red) and bulk (blue) emissions. The spectra were fitted by four Doniach−Sunjic peaks with the same Shirley background, width, and asymmetry for the surface and the bulk components, all convoluted with a Gaussian line to account for the experimental resolution. After 45 s of Gd deposition, the intensity of the surface component is largely reduced while the other nonsurface emissions increase. We attribute the remaining surface emission to uncovered, clean Au patches, which occupy about 31% of the surface. This result is consistent with angle-resolved photoemission measurements of the Au surface state, whose intensity drops to one-third with respect to the Gd-free surface value. The increasing contribution of the nonsurface Au 4f component is assigned to the formation of the Gd−Au compound. Its corresponding Au 4f emission would be thus located at a similar energy to that of the Au crystal. The total intensity of all 4f components after 45 s Gd deposition is reduced with respect to pure Au, as expected from the attenuation effect of Gd atoms. In order to test the stoichiometry of the compound during the reactive epitaxy, we perform a more than 10 times larger, 8 min Gd deposition, which gives rise to a few layers deep Gd−Au compound and, hence, a 4f emission that can be entirely attributed to the compound. In fact, we observe that after 8 min deposition the 4f surface component is completely quenched, whereas the overall intensity of the 4f emission becomes exactly two-thirds of the clean Au 4f emission, that is, the ratio expected for a homogeneous 1: 2 GdAu stoichiometry.

All of the results obtained with several experimental techniques agree in the identification of the Gd−Au structure as a two-dimensional $GdAu_2$ surface compound with an atomic density close to the [110] plane of bulk $GdAu_2$[25] on top of the Au(111) surface. A model of this structure is shown in Figure 3d, where the alloy unit cell is sketched. The atoms of the topmost layer form a honeycomb lattice with a nearest neighbor distance of 3.13 Å. The six-fold coordinated central sites of this lattice are occupied by Gd atoms while the others are Au atoms. The Moiré contrast is induced by the superposition of the $GdAu_2$ lattice on top of the Au substrate since the overlayer in-plane lattice constant (d_{Gd-Au} = 3.13 Å) is larger than the one of Au(111). The $GdAu_2$/Au(111) coincidence lattice corresponds to (12 × 12) alloy units (with 96 Au and 48 Gd atoms per Moiré unit cell) on top of (13 × 13) substrate units (with 169 Au atoms), that is, $d_{Moiré} = 12 \times 3.13$ Å = 37.6 Å. In this mixed layer (1 ML $GdAu_2$ surface compound), in the entire (12 × 12) unit cell, the density of Au atoms with re-

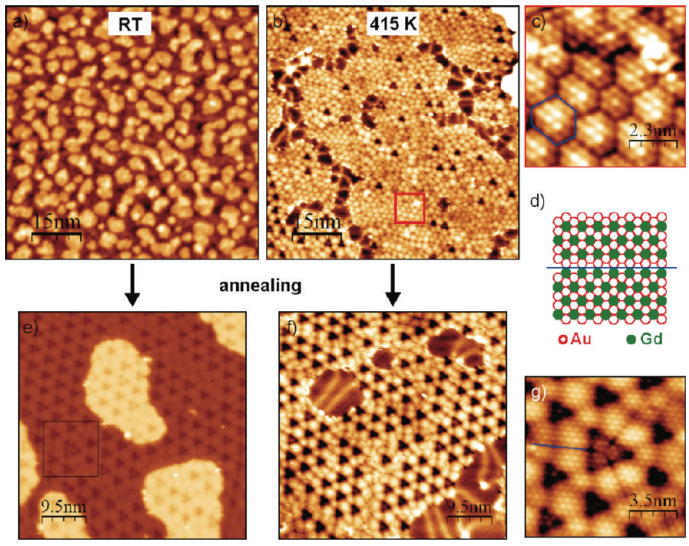

Figure 6. (a) Island formation after 2.5 min Gd deposition onto Au(111) at rt. (b) Deposition of Gd at 415 K (2 min, <0.5 ML) results in the formation of a hexagonal atomic network, coexisting with some trigon units, DL and triangles of the Gd−Au compound. (c) Atomically resolved STM image in the area defined by the square in (b) of the network of hexagonal clusters. An atomic model of the boundary between them (blue line) is pictured in (d). The assignment (red, green) of Au and Gd atoms is arbitrary. (e,f) $GdAu_2$ Moiré structure formed after 15 min annealing to 415 K of the surfaces in (a) and (b), respectively. In (e), some islands of a second $GdAu_2$ layer are present, while in (f), the surface is only partially covered by the alloy. (g) Zoom image in (e) showing a defect in the $GdAu_2$ film. The defect (blue line) can be interpreted as an exchanged atomic species in the surface compound (d). (a) $I_t = 0.3$ nA, $V_s = -1$ V; (b) $I_t = 0.3$ nA, $V_s = -0.1$ V; (c) $I_t = 0.3$ nA, $V_s = -0.1$ V; (e) $I_t = 0.3$ nA, $V_s = -0.8$ V; (f) $I_t = 0.17$ nA, $V_s = -1$ V; (g) $I_t = 0.3$ nA, $V_s = -0.76$ V.

spect to an unreconstructed Au(111) substrate is 0.57 ML, while the density of Gd atoms is 0.28 ML. The corrugation of ~0.6 Å observed in the Moiré is due to the modulation of the vertical position of the surface atoms which occupy within the unit cell different adsorption sites with respect to the substrate. This vertical modulation is close to the nominal variation (0.53 Å) from top to hollow positions in the Au(111) surface, that is, $\{[(1/\sqrt{2}) - (1/\sqrt{3})] \times a_{Au}\}$ with $a_{Au} = 4.08$ Å.[26] A careful analysis of large-scale atomically resolved STM images shows that small deviations from the 12 on 13 scheme can occur, suggesting that rather than a coincidence lattice in total an incommensurate layer is formed.

The surface structure of this $GdAu_2$ compound presents striking analogies to the $NaAu_2$ surface alloy.[16,27] Similar to $GdAu_2$, it forms when a Au(111) substrate covered by 0.5 ML of Na is flashed to 600 K. STM images in $NaAu_2$ reveal a hexagonal atomic lattice oriented along the $[\bar{1}\bar{1}2]$ direction, with nearest neighboring equivalent species at 5.4 Å, and a large-scale Moiré pattern of 38 Å periodicity.

In order to characterize the growth of the compound, we exposed the Au(111) surface to Gd at temperatures lower than 550 K. Figure 6a shows islands which form after 2.5 min deposition of Gd at room temperature and occupy half of the substrate surface. The islands have irregular shapes and have a height of ~2.2−3 Å. They probably correspond to a single Gd(0001) layer (with nominal step height of 2.89 Å),[26] but since no herringbone reconstruction can be identified in the areas between the islands, we cannot exclude that they also incorporate Au atoms. A deposition temperature of 415 K of the Au(111) surface is already enough to avoid Gd clustering and island formation. Figure 6b shows the outcome of the deposition of 2 min Gd at 415 K. Three kinds of structures can be found on the surface: the DL typical of the trigons, some triangles resembling those of the $GdAu_2$ Moiré, and a network of hexagonally packed atomic clusters, well visible in Figure 6c. In this last structure, again, STM images show only one atomic species in a hexagonal lattice with a nearest neighbor distance of $d = 5.5-6.2$ Å, suggesting that the surface is formed locally as a $GdAu_2$ compound. Nevertheless, the surface layer is not homogeneous because it is divided in hexagonal groups of atoms shifted with respect to the neighbors. The number of imaged atoms in the regular groups occurring more frequently is 7, 10, and 12. Figure 6d schematically pictures the boundary between each hexagonal unit (blue line). The atomic arrangement can be interpreted as a local atomic fault in the $GdAu_2$ layer due to an interchange between Gd and Au species, such that, across the boundary, atoms appear aligned along the non-close-packed direction and shifted in the closed-packed one, as imaged by STM. In the places of the surface (Figure 6b) where Moiré triangles form, the atomic layer is again continuous and free from any atomic shift.

A long (15 min) annealing to 415 K of the two preparations induces the formation of the $GdAu_2$ compound (Figure 6e,f). The rt islands and the hexagonal network disappear. The Gd−Au Moiré is not as regular as when it is grown directly at higher temperature (550 K), but undoubtedly the structure is the same. Figure 6g shows a typical defect that can be encountered in the $GdAu_2$ surface layer, of the same type as the one modeled in Figure 6d.

Besides the temperature dependence on the Gd deposition of the compound formation, we investigated the growth of multilayers. It is not trivial to assign the exact value for the thickness of the layers due to Gd diffusion inside the Au bulk. To get a rough idea on the Gd coverage, we can refer to Figure 6a, where the surface was exposed to Gd for 2.5 min at rt, resulting in a Au(111) surface half covered. Figure 7 shows a series of STM images measured after exposure at 550 K to increasing amounts of Gd; Figure 7a corresponds

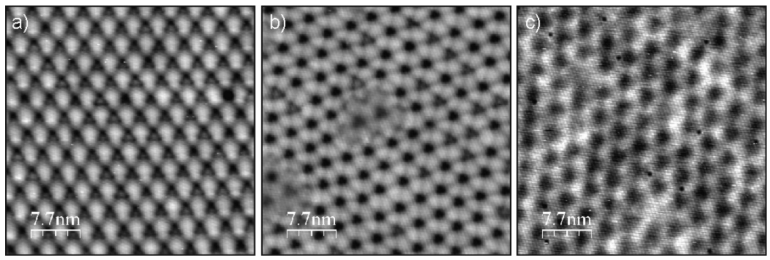

Figure 7. STM images of the $GdAu_2$ surface alloy measured after exposure to Gd at 550 K for 2.5 min (a), for 10 min (b), and for 20 min (c). In thin layers, the overstructure is characterized only by triangles (a), as thickness is increased, by circles (b) up to gradual disappearance of the Moiré (c). (a) $I_t = 0.3$ nA, $V_s = -0.65$ V; (b) $I_t = 0.3$ nA, $V_s = 0.3$ V; (c) $I_t = 0.3$ nA, $V_s = -1$ V.

to 2.5 min Gd exposure, Figure 7b to 10 min, and Figure 7c to 20 min.

For thin layers (Figure 7a), the surface is characterized by the $GdAu_2$ alloy structure described above. With an increased thickness (exposure longer than 5 min), the appearance of triangles gives place to circles in the Moiré, as already observed for 1 and 2 ML of Ag/Cu(111).[22] On thicker layers, the overstructure is characterized by areas with a different STM contrast where the Moiré periodicity is locally broken (Figure 7b) or there are some missing unit cells. Since the top layer is made of a continuous lattice, these defects are probably growing on lower layers eventually poor in Au, where a complete surface compound was not formed. For films of larger Gd thickness (Figure 7c), the Moiré pattern corrugation gets weaker (0.10 ± 0.05 Å) due to the larger distance from the Au substrate, but the top atomic layer preserves its lattice spacing of 5.5 ± 0.3 Å.

Co Nanodots Arrays. The fabrication of robust ultrahigh density lattices of magnetic dots at rt is a big challenge. One of the most straightforward alternatives is the self-organized growth using template surfaces. This approach has already given successful results with the employment of different kinds of templates as strain relief patterns,[28] vicinal surfaces,[29] thin insulating films on metals,[30] and recently metal-organic networks.[31]

Up to now, the state-of-the-art system showing a record density of magnetic islands (26 Terabits/in^2, namely, 4.2×10^{16}/m^2)[29] is Co on Au(788). In this work, we have also tested the trigons network and the $GdAu_2$ surface compound as templates to grow Co nanostructures. As we show below, these Gd−Au surface phases, in particular, the $GdAu_2$ surface compound, represent an important step forward in the research of technologically exploitable nanotemplates.

Figure 8 shows four examples of Co growth on different Au templates: Au(111) (Figure 8a), the Gd/Au(111) trigons (Figure 8b), Au(25 27 27) (Figure 8c), and the $GdAu_2$ surface compound (Figure 8d), as indicated. For this purpose, Co was evaporated onto the Au-derived substrates using a deposition rate of 0.8 Å/min. In Figure 8a, the Au(111) was exposed for 35 s to Co at rt, resulting in a Co surface coverage of ~0.5 Å; in Figure 8b, the Co surface coverage is ~0.6 Å (45 s at rt); in Figure 8c, it corresponds to ~0.5 Å (35 s at 170 K); and in Figure 8d, the Co coverage is ~6 Å (480 s at rt).

On Au(111), Co grows preferentially at the elbows of the HB reconstruction, thus creating an almost rectangular pattern. Previous studies showed that Co islands form in a two-step process: at first, the nucleation starts at the pinch-in and pinch-out dislocations *via* a place exchange process of Au atoms in the substrate with Co adatoms; then bigger and bigger Co particles develop around the substitutional Co atoms.[32,33] Figure 8a displays an ordered array of Co islands, two atomic Co layers high (4 Å), grown at rt on Au(111), with a 7% covered surface. By means of this template, it is possible to reach a surface density of Co islands of 5.5 Teradots/in^2. A similar Co network can be grown on vicinal Au(111) surfaces with B-type steps (*i.e.*, with {111}-oriented microfacets). In such surfaces, nucleation of Co takes place at the crossing of the DL of the HB recon-

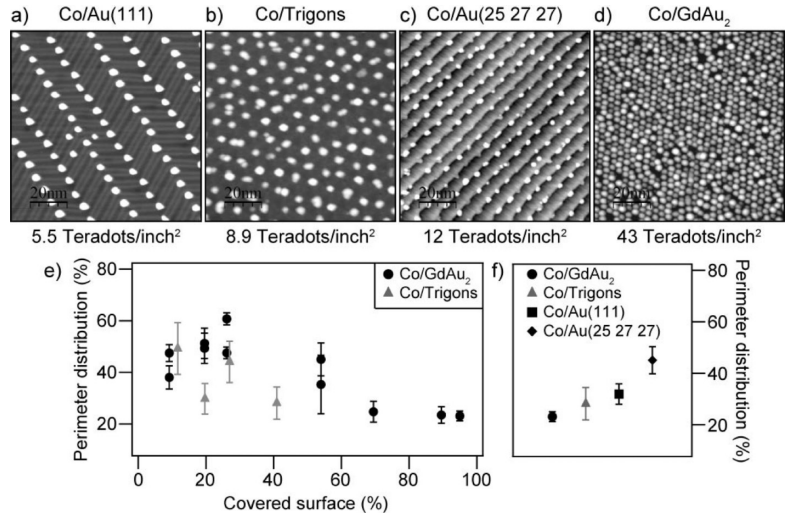

Figure 8. (a−d) STM images (100 × 100 nm^2) showing the growth and packing of Co nanoislands on different Au(111)-derived nanotemplates as indicated on the top of each image. The images are ordered with respect to their corresponding Co dot density per in^2, from the least dense (a) on the left to the most dense (d) on the right. (e) Dispersion plot showing the "perimeter distribution" of Co nanoislands or dots grown on the trigons and on the $GdAu_2$ templates as a function of the covered surface. The perimeter distribution is defined as the ratio between the hwhm of the Gaussian line that best fits the perimeter distribution histogram of the Co islands and its center. (f) Best values for the perimeter distribution obtained for Co growth on the templates in (a−d). (a) $I_t = 0.5$ nA, $V_s = -1$ V; (b) $I_t = 0.1$ nA, $V_s = -1$ V; (c) $I_t = 0.3$ nA, $V_s = -1$ V; (d) $I_t = 0.3$ nA, $V_s = -1$ V.

struction and the steps.[29,34] Figure 8c shows an example of Co growth (at 170 K) on Au(25 27 27), a surface with 2° miscut angle with respect to Au(111).[28] There, Co particles regularly arrange into a long-range ordered rectangular superlattice with a unit cell of (6.5 × 7.2) ± 0.2 nm^2 and a surface density of 12 Teradots/in^2, much higher than on Au(111). Nevertheless, denser Co particle arrays can be obtained just by decreasing the step size (*i.e.*, increasing the miscut angle), as in the Au(788) surface.[29]

The surface reconstruction of Au(111) and its B-type vicinals drives the spontaneous formation of open rectangular networks of adsorbed nanostructures whose density is limited by the HB periodicity and the minimum step size at which the HB forms.[35] A higher number of nucleation centers on Au(111) templates can be induced by high-temperature deposition of Gd atoms. In this way, we are able to change the rectangular symmetry of the surface template to a more packed hexagonal one. Figure 8b shows an example of Co growth at rt on a trigons network and Figure 8d on the $GdAu_2$ Moiré. Co clusters preferentially nucleate on top of the nodes of the network of trigons, filling each trigon unit, and maintaining the average distance of 9.0 ± 0.6 nm. For low coverages, the nanodots have a maximum height of 2.2 ± 0.2 Å corresponding to a single Co(0001) layer (2.05 Å); at higher coverages, double-layer nanoislands 4.5 ± 0.2 Å high grow at the expense of the single-layer ones. The hexagonal array of Co islands in Figure 8b shows a density of 8.9 Teradots/in.^{2}, higher than the one of Co on Au(111) but lower than the one obtained at B-type Au(111) vicinals.

Among all of the cases presented so far, the best example is undoubtedly represented by the $GdAu_2$ template where we can reach record Co nanodot densities exceeding the 43 Teradots/in^2 value shown in Figure 8d.[36] Co dots follow faithfully the pattern given by the underlying Moiré maintaining its distance of 3.8 ± 0.2 nm. They nucleate on top of the triangular areas defined by the overstructure, those corresponding to the *on top* sites of the Au substrate as in the case of trigons. Very interestingly, optimum growth conditions (*i.e.*, high density and homogeneous nucleation on Moiré adsorption sites) are achieved at rt.[36] We direct the reader to ref 36 for further details on the growth and magnetic properties of these Co nanodot arrays.

Template-guided vapor deposition epitaxy is limited on one side by the presence of missing bits (filling rate) and on the other side by the resulting nanodot size distribution. In magnetic systems, the size distribution gives rise to magnetic anisotropy broadening, which affects the performance of the write−read devices. In Co nanodot arrays of Figure 8, we quantified the size distribution through the dot perimeter. For each sample preparation, we measured the perimeter distribution histogram resulting from several STM images by means of Gaussian fits. We define as perimeter distribution the ratio between the hwhm and the center value of the fitted Gaussian line obtained. In the case of Co/trigons, as expected, the perimeter of the islands increases with covered surface and its distribution varies between 28% (Figure 8e), in the best case of homogeneously sized islands (Figure 8b), and 49%, at low coverages. On the $GdAu_2$ surface alloy at low coverages, Co growth is bimodal, giving rise to a broader perimeter distribution in Figure 8e. At higher coverages, such a growth mode is suppressed and equally sized dots fill up the surface. The latter case is the one shown in Figure 8d. With a total coverage of 6 Å, the surface appears completely covered with four monolayer thick, roundly shaped Co nanodots. These exhibit a rather uniform perimeter of 12.3 ± 2.8 nm, which corresponds to the maximum diameter of 3.9 nm that the hexagonal Moiré superlattice can host.

Figure 8f allows us to judge the quality of the Co dots grown on the different Au(111)-derived templates shown in Figure 8a−d. Undoubtedly, Co dots grow with the most uniform size on the $GdAu_2$ surface where we obtain in the best case the low value of 23% for the perimeter distribution. Such a value is as good as the one obtained for the size distribution of Co particles on Au(788),[29] which ranges between 20 and 32% depending on the Co coverage.

CONCLUSIONS

In conclusion, we investigated the high-temperature (550 K) growth of Gd on Au(111) for a wide range of coverages. We discovered the formation of two stable and ordered equilibrium surface phases: a network of trigons at low coverages and a highly periodic $GdAu_2$ surface compound. Combined STM, LEED, and XPS studies allowed identifying their stoichiometry and atomic structure. Both phases can be used as nanotemplates to grow arrays of metal nanodots as shown in the case of Co. Among all of the cases reported so far of Co growth on Au(111)-derived templates, the ordering of Co on the $GdAu_2$ nanopatterned surface is the best. We can reach Co nanodot arrays homogeneously sized (23% perimeter distribution) and with ultrahigh densities up to 43 Teradots/in^2.

METHODS

Samples have been prepared in an ultrahigh vacuum (UHV) chamber at a base pressure of 7 × 10^{-11} mbar, equipped with a variable-temperature scanning tunneling microscope (VT STM XA, Omicron) and low-energy electron diffraction optics (LEED). Au(111) single crystals and commercial Au(111) films, 150 nm thick *ex situ* deposited on mica, were used as substrates. The samples were cleaned by repeated cycles of Ar^+ sputtering and annealing to 800 K until achievement of an ordered herringbone reconstruction. Gd was evaporated by molecular beam epitaxy

on the clean Au(111) surfaces with a deposition rate of 2 Å/min, as estimated from a quartz microbalance. The substrate temperature during Gd evaporation was 550 K with a vacuum pressure below 1×10^{-9} mbar. After deposition, the samples were immediately cooled to 300 K for STM measurements. The STM data here presented were measured with W and Pt/Ir tips and have been analyzed using the WSxM software.[37] Co was evaporated by molecular beam epitaxy using a commercial high-voltage electron-beam evaporator with a deposition rate of around 0.8 Å/min, substrate temperature of 300 K, and a vacuum pressure below 6×10^{-10} mbar.

X-ray photoelectron spectroscopy measurements were carried out at the PGM beamline of the Synchrotron Radiation Center (SRC) at the University of Wisconsin (USA).

Acknowledgment. This work was financed by the Basque Government (Nanotron, IT-257-07), the Spanish Ministry of Science and Innovation (MAT2007-63083). The Synchrotron Radiation Center is funded by the National Science Foundation (Award No. DMR-0084402). We also thank Prof. Thomas Greber from the Physics Institute, University of Zurich, for the collaboration on some data acquisition and analysis.

REFERENCES AND NOTES

1. Barth, J. V.; Costantini, G.; Kern, K. Engineering Atomic and Molecular Nanostructures at Surfaces. *Nature* **2005**, *437*, 671–679.
2. Becker, C.; Wandelt, K. Two-Dimensional Templates. *Top. Curr. Chem.* **2009**, *287*, 45–86.
3. Prod'homme, P.; Maroun, F.; Cortès, R.; Allongue, P. Electrochemical Growth of Ultraflat Au(111) Epitaxial Buffer Layers on H-Si(111). *Appl. Phys. Lett.* **2008**, *93*, 171901.
4. Cagnon, L.; Devolder, T.; Cortès, R.; Morrone, A.; Schmidt, J. E.; Chappert, C.; Allongue, P. Enhanced Interface Perpendicular Magnetic Anisotropy in Electrodeposited Co/Au(111) Layers. *Phys. Rev. B* **2001**, *63*, 104419.
5. Love, J. C.; Estroff, L. A.; Kriebel, J. K.; Nuzzo, R. G.; Whitesides, G. M. Self-Assembled Monolayers of Thiolates on Metals as a Form of Nanotechnology. *Chem. Rev.* **2005**, *105*, 1103–1169.
6. Barth, J. V.; Brune, H.; Ertl, G.; Behm, R. J. Scanning Tunneling Microscopy Observations on the Reconstructed Au(111) Surface: Atomic Structure, Long-Range Superstructure, Rotational Domains, and Surface Defects. *Phys. Rev. B* **1990**, *42*, 9307–9318.
7. Harten, U.; Lahee, A. M.; Toennies, J. P.; Wöll, C. Observation of a Soliton Reconstruction of Au(111) by High-Resolution Helium-Atom Diffraction. *Phys. Rev. Lett.* **1985**, *54*, 2619–2622.
8. Sandy, A. R.; Mochrie, S. G. J.; Zehner, D. M.; Huang, K. G.; Gibbs, D. Structure and Phases of the Au(111) Surface: X-ray-Scattering Measurements. *Phys. Rev. B* **1991**, *43*, 4667–4687.
9. Yin, F.; Palmer, R.; Guo, Q. Nanoscale Surface Recrystallization Driven by Localized Electric Field. *Phys. Rev. B* **2006**, *73*, 073405.
10. Wang, Y.; Hush, N. S.; Reimers, J. R. Simulation of the Au(111)-$(22 \times \sqrt{3})$ Surface Reconstruction. *Phys. Rev. B* **2007**, *75*, 233416.
11. Cullen, W. G.; First, P. N. Island Shapes and Intermixing for Submonolayer Nickel on Au(111). *Surf. Sci.* **1999**, *420*, 53–64.
12. Narasimhan, S.; Vanderbilt, D. Elastic Stress Domains and the Herringbone Reconstruction on Au(111). *Phys. Rev. Lett.* **1992**, *69*, 1564–1567.
13. Kowalczyk, P.; Kozlowski, W.; Klusek, Z.; Olejniczak, W.; Datta, P. K. STM Studies of the Reconstructed Au(111) Thin-Film at Elevated Temperatures. *Appl. Surf. Sci.* **2007**, *253*, 4715–4720.
14. Fischer, B.; Barth, J. V.; Fricke, A.; Nedelmann, L.; Kern, K. Growth and Surface Alloying of Al on Au(111) at Room Temperature. *Surf. Sci.* **2008**, *602*, L115–L117.
15. Barth, J. V.; Behm, R. J.; Ertl, G. Mesoscopic Structural Transformations of the Au(111) Surface Induced by Alkali Metal Adsorption. *Surf. Sci. Lett.* **1994**, *302*, L319–L324.
16. Barth, J. V.; Behm, R. J.; Ertl, G. Adsorption, Surface Reconstruction and Alloy Formation in the Na/Au(111) System. *Surf. Sci.* **1995**, *341*, 62–91.
17. Rossel, F.; Brodard, P.; Patthey, F.; Richardson, N. V.; Schneider, W. D. Modified Herringbone Reconstruction on Au(111) Induced by Self-Assembled Azure A Islands. *Surf. Sci. Lett.* **2008**, *602*, L115–L117.
18. Pushpa, R.; Narasimhan, S. Reconstruction of Pt(111) and Domain Patterns on Close-Packed Metal Surfaces. *Phys. Rev. B* **2003**, *67*, 205418.
19. Hohage, M.; Michely, T.; Comsa, G. Pt(111) Network Reconstruction: Structure, Growth and Decay. *Surf. Sci.* **1995**, *337*, 249–267.
20. Carter, C. B.; Hwang, R. Q. Dislocations and the Reconstruction of (111) fcc Metal Surfaces. *Phys. Rev. B* **1995**, *51*, 4730–4733.
21. Bendounan, A.; Cercellier, H.; Fagot-Revurat, Y.; Kierren, B.; Yu Yurov, V.; Malterre, D. Modification of Schockley States Induced by Surface Reconstruction in Epitaxial Ag Films on Cu(111). *Phys. Rev. B* **2003**, *67*, 165412.
22. Schiller, F.; Cordón, J.; Vyalikh, D.; Rubio, A.; Ortega, J. E. Fermi Gap Stabilization of an Incommensurate Two-Dimensional Superstructure. *Phys. Rev. Lett.* **2005**, *94*, 016103.
23. Jacobsen, J.; Nielsen, L. P.; Besenbacher, F.; Stensgaard, I.; Lægsgaard, E.; Rasmussen, T.; Jacobsen, K. W.; Nørskov, J. K. Atomic-Scale Determination of Misfit Dislocation Loops at Metal−Metal Interfaces. *Phys. Rev. Lett.* **1995**, *75*, 489–492.
24. Ling, W. L.; Hamilton, J. C.; Thürmer, K.; De la Figuera, J.; Hwang, R. Q.; Carter, C. B.; Bartelt, N. C.; McCarty, K. F. Herringbone and Triangular Patterns of Dislocations in Ag, Au, and AgAu Alloy Films on Ru(0001). *Surf. Sci.* **2006**, *600*, 1735–1757.
25. Watson, R. E.; Weinert, M.; Davenport, J. W. Structural Stabilities of Layered Materials: Pt-Ta. *Phys. Rev. B* **1987**, *35*, 9284–9286.
26. Ashcroft, N. W.; Mermin, N. D. *Solid State Physics*; Saunders College Publishers: Philadelphia, PA, 1976.
27. Barth, J. V.; Brune, H.; Schuster, R.; Ertl, G. Intermixing and Two-Dimensional Alloy Formation in the Na/Au(111) System. *Surf. Sci. Lett.* **1993**, *292*, L769–L774.
28. Brune, H.; Giovannini, M.; Bromann, K.; Kern, K. Self-Organized Growth of Nanostructure Arrays on Strain-Relief Patterns. *Nature* **1998**, *394*, 451–453.
29. Weiss, N.; Cren, T.; Epple, M.; Rusponi, S.; Baudot, G.; Rohart, S.; Tejeda, A.; Repain, V.; Rousset, S.; Ohresser, P.; Scheurer, F.; Bencok, P.; Brune, H. Uniform Magnetic Properties for an Ultrahigh-Density Lattice of Noninteracting Co Nanostructures. *Phys. Rev. Lett.* **2005**, *95*, 157204.
30. Schmid, M.; Kresse, G.; Buchsbaum, A.; Napetschnig, E.; Gritschneder, S.; Reichling, M.; Varga, P. Nanotemplate with Holes: Ultrathin Alumina on $Ni_3Al(111)$. *Phys. Rev. Lett.* **2007**, *99*, 196104–196107.
31. Decker, R.; Schlickum, U.; Klappenberger, F.; Zoppellaro, G.; Klyatskaya, S.; Ruben, M.; Barth, J. V.; Brune, H. Using Metal-Organic Templates to Steer the Growth of Fe and Co Nanoclusters. *Appl. Phys. Lett.* **2008**, *93*, 243102.
32. Voigtländer, B.; Meyer, G.; Amer, N. M. Epitaxial Growth of Thin Magnetic Cobalt Films on Au(111) Studied by Scanning Tunneling Microscopy. *Phys. Rev. B* **1991**, *44*, 10354–10357.
33. Meyer, J. A.; Baikie, I. D.; Kopatzki, E.; Behm, R. J. Preferential Island Nucleation at the Elbows of the Au(111) Herringbone Reconstruction through Place Exchange. *Surf. Sci.* **1996**, *365*, L647–L651.
34. Repain, V.; Rohart, S.; Girard, Y.; Tejeda, A.; Rousset, S. Building Uniform Long-Range Ordered Nanostructures on a Surface by Nucleation on a Point Defect Array. *J. Phys.: Condens. Matter* **2006**, S17–S26.

35. Corso, M.; Schiller, F.; Fernández, L.; Cordón, J.; Ortega, J. E. Electronic States in Faceted Au(111) Studied with Curved Crystal Surfaces. *J. Phys.: Condens. Matter* **2009**, *21*, 353001.
36. Fernández, L.; Corso, M.; Schiller, F.; Ilyn, M.; Holder, M.; Ortega, J. E. Self-Organized Growth of High Density Magnetic Co Nanodot Arrays on a Moiré Template. *Appl. Phys. Lett.* **2010**, *96*, 013107.
37. Horcas, I.; Fernández, R.; Gómez-Rodriguez, J. M.; Colchero, J.; Gómez-Herrero, J.; Baro, A. M. WSXM: A Software for Scanning Probe Microscopy and a Tool for Nanotechnology. *Rev. Sci. Instrum.* **2007**, *78*, 13705.